CMS Physics Analysis Summary

Contact: cms-pag-conveners-higgs@cern.ch 2015/10/12

Search for Higgs Decays to New Light Bosons in Boosted Tau Final States

The CMS Collaboration

Abstract

A search for non-standard decays of a Standard Model-like Higgs boson to pairs of light bosons, as predicted in models with extended Higgs sectors, is presented. In two Higgs doublet models, including the next-to-minimal supersymmetric standard model, the Higgs can decay into a pair of light scalars h or pseudoscalars a. In this search, the gluon fusion, W and Z associated Higgs, and vector boson fusion production channels for the Higgs are all considered, and the decay $\mathrm{H} \to \mathrm{aa}(\mathrm{hh})$ with $\mathrm{a}(\mathrm{h}) \to \tau\tau$ is reconstructed from the tau decay products. The final state is characterized by one isolated high p_{T} muon plus at least one highly boosted pair of taus, of which one of the taus is required to decay to a muon. Using 19.7 fb^{-1} of 8 TeV center of mass pp collision data recorded by the Compact Muon Solenoid experiment at the Large Hadron Collider, a counting experiment is performed in a region of high di-tau invariant mass. No excess of events above the Standard Model backgrounds is found, and upper limits are set on the branching ratio $BR(\mathrm{H} \to \mathrm{aa/hh})BR^2(\mathrm{a/h} \to \tau\tau)$.

1 Introduction

Studies [1–3] of the properties of the recently discovered Higgs-like particle H with mass $\sim$125.5 GeV/c^2 [4, 5] already significantly constrain a number of theoretical physics models incorporating Higgs sectors extending beyond the standard model (SM). However, current analyses do not cover all theoretically possible H decay modes; a survey of existing LHC and Tevatron data [6] finds that at 95% C.L. the branching ratio to as-yet-unseen decay modes U cannot exceed 21% for an H with completely SM-like couplings to quarks, leptons and vector bosons, but can be as high as 39% in the case where the Higgs sector contains only doublets and singlets and the above H couplings are otherwise free to vary with respect to their standard model values.

Given the allowed branching ratio for unseen H decays, it is interesting to explore the important possibility [7, 8] that decays of the type $\mathrm{H} \to \mathrm{aa}$ or $\mathrm{H} \to \mathrm{hh}$ are present [9, 10], where $\mathrm{a(h)}$ is a lighter pseudoscalar(scalar) Higgs boson. Such decays are possible in the context of various extensions of the standard model, including two-Higgs-doublet models (2HDM), the next-to-minimal supersymmetric standard model (NMSSM), and purely Higgs-sector models containing additional Higgs fields, but are not possible in the CP-conserving minimal supersymmetric standard model (MSSM) due to the tightly constrained nature of the Higgs sector in combination with experimental constraints. 2HDM studies that consider the possible decays of the observed standard model-like Higgs to a pair of lighter Higgs bosons include Refs. [10–18]. Studies in the NMSSM or NMSSM-like context include Refs. [10, 19–22] and studies in the general case of adding a singlet field to the standard model or the 2HDM can be found in Refs. [10, 23, 24].

In all of the models listed above (aside from the CP-conserving MSSM), it is possible that the lightest Higgs (pseudo)scalar is much lighter than the SM-like Higgs boson. If the light Higgs is a scalar then the SM-like Higgs should be identified with the second lightest scalar of the model. In the specific case of the NMSSM a light a arises naturally in the limit of a $U(1)_R$ symmetry of the model and the SM-like Higgs can be either the lightest or second lightest scalar. Experimental limits from LEP set stringent constraints on the mass of the lightest scalar h if it is doublet-dominated, but if the h is singlet-dominated, these constraints relax and significantly lower masses are possible as well (see [20] and [25]). In general, these models allow for large $BR(\mathrm{H} \to \mathrm{hh})$ or $BR(\mathrm{H} \to \mathrm{aa})$ when kinematically allowed, but existing experimental measurements constrain the allowed parameter space for these types of models to model points with $BR(\mathrm{H} \to \mathrm{aa}) + BR(\mathrm{H} \to \mathrm{hh}) < 39\%$. Various searches for different scenarios involving light scalars or light pseudoscalars have been performed; examples from the CMS experiment are a search for scalar Higgses in the mass range 30-100 GeV/c^2 [26] and another that probes a pseudoscalar Higgs mass range as low as 0.25-3.55 GeV/c^2 [27].

A direct constraint of relevance is the previous CMS result [28] (based on Ref. [29]), which places limits on $\sigma(\mathrm{pp} \to \mathrm{a})BR(\mathrm{a} \to \mu\mu)$ of order 2$-$6 pb in the mass range from 5$-$14 GeV/c^2, excluding the upsilon resonance region. This result significantly constrains the NMSSM $\cos\theta_A$ mixing angle factor defining the mass eigenstate: $\mathrm{a} = \cos\theta_A \mathrm{a}_{\mathrm{MSSM}} + \sin\theta_A \mathrm{a}_{\mathrm{S}}$, where $\mathrm{a}_{\mathrm{MSSM}}$ is the MSSM-like pseudoscalar of the NMSSM and a_{S} is the singlet pseudoscalar of the NMSSM. The constraints on $|\cos\theta_A|$ are especially strong at large $\tan\beta$. In the case of the CP-conserving 2HDM Type II models with $m_{\mathrm{H}} \sim 125.5$ GeV/c^2, many otherwise acceptable parameter choices yielding $m_{\mathrm{a}} \leq 14$ GeV/c^2 are ruled out by the Ref. [28] limit (see Ref. [18]). However, in both cases large $BR(\mathrm{H} \to \mathrm{aa})$ and/or $BR(\mathrm{H} \to \mathrm{hh})$ remain possible.

This analysis considers 4τ final states arising from $\mathrm{H} \to \mathrm{aa} \to 4\tau$ or $\mathrm{H} \to \mathrm{hh} \to 4\tau$, where the H is produced in association with a W or Z boson decaying leptonically, via gluon fusion, or

via vector boson fusion (VBF). The a or h mass is studied in the range 5−15 GeV/c^2. For $m_{a/h} \lesssim 11$ GeV/c^2, $BR(a/h \to \tau\tau)$ is generically large, while for $m_{a/h} \gtrsim 11$ GeV/c^2, decays to bottom quarks become dominant but there is still a small $BR(a/h \to \tau\tau)$. For example, Ref. [10] finds model points with $BR(h \to \tau\tau) \sim 90(7)\%$ for $m_h \lesssim(\gtrsim) 10$ GeV/c^2. The large boost of the a or h causes its decay products to overlap, necessitating the use of a special boosted di-tau pair reconstruction technique based on the specific decay $a/h \to \tau_\mu \tau_X$. This analysis is performed in two search regions based on the transverse mass of a high p_T muon and the event missing transverse energy, defined to distinguish between the WH production mode and modes without significant missing transverse energy.

2 CMS Event Reconstruction

The central feature of the Compact Muon Solenoid (CMS) apparatus is a superconducting solenoid of 6 m internal diameter, providing a magnetic field of 3.8 T. Within the superconducting solenoid volume are a silicon pixel and strip tracker, a lead tungstate crystal electromagnetic calorimeter (ECAL), and a brass/scintillator hadron calorimeter (HCAL), each composed of a barrel and two endcap sections. Muons are measured in gas-ionization detectors embedded in the steel flux-return yoke outside the solenoid. Extensive forward calorimetry complements the coverage provided by the barrel and endcap detectors. A more detailed description can be found in Ref. [30].

This analysis makes use of the CMS particle flow event reconstruction. The particle-flow event reconstruction consists in reconstructing and identifying each single particle with an optimised combination of all subdetector information. The energy of photons is directly obtained from the ECAL measurement, corrected for zero-suppression effects. The energy of electrons is determined from a combination of the track momentum at the main interaction vertex, the corresponding ECAL cluster energy, and the energy sum of all bremsstrahlung photons attached to the track. The energy of muons is obtained from the corresponding track momentum. The energy of charged hadrons is determined from a combination of the track momentum and the corresponding ECAL and HCAL energy, corrected for zero-suppression effects, and calibrated for the nonlinear response of the calorimeters. Finally the energy of neutral hadrons is obtained from the corresponding calibrated ECAL and HCAL energy.

Simulated events are used in studies supporting the analysis methods and background determination, as well as to model the Higgs decay to light (pseudo)scalars and subsequent decay to taus. Simulated samples of Drell-Yan, W, $t\bar{t}$, and di-boson events use MADGRAPH [31] for the matrix element calculation; PYTHIA [32] for parton showering, hadronization, and most particle decays; and TAUOLA [33] specifically for tau decays. WH, ggH, ZH, and vector boson fusion (VBF) signal samples are generated with PYTHIA using its built-in 2HDM functionality with $H \to aa$, $a \to \tau\tau$. For the WH and ggH production modes, samples are generated with m_a = 5, 7, 9, 11, 13, 15 GeV/c^2. For the ZH and VBF modes, only samples with m_a = 9 GeV/c^2 are generated. The standard CMS detector simulation (based on GEANT [34]) and event reconstruction is applied to all signal and background simulations.

Two sets of muon identification criteria are used in this analysis. The "trigger muon" μ_{trg} is required to have $p_T > 25$ GeV/c, $|\eta| < 2.1$, be well reconstructed in both the muon chambers and the silicon tracker, have a high quality track fit, and be consistent with origination from the primary pp interaction in the event. In addition, it is required to be isolated from other photons, hadrons, and leptons in the detector. Isolation from photons and hadrons is enforced by requiring that the ratio of the sum of the transverse energy (corrected for the presence of multiple low p_T pp interactions per event, or pileup) of the reconstructed photons and hadrons

in a cone with radius $\Delta R = \sqrt{\Delta\eta^2 + \Delta\phi^2} = 0.4$ around the muon to the muon momentum is less than 0.12. To be isolated from other leptons, the trigger muon is required not to overlap with any identified electron ($p_T > 7$ GeV/c, $|\eta| < 2.5$, cf. Ref. [35]), muon ($p_T > 5$ GeV/c, $|\eta| < 2.4$, passing "tau muon" criteria below), or tau ($p_T > 10$ GeV/c, $|\eta| < 2.3$, passing modified HPS criteria below) within $\Delta R = 0.4$.

The identification criteria for the "tau muon" τ_μ require that it have $p_T > 5$ GeV/c, $|\eta| < 2.4$, be well reconstructed in the silicon tracker, have a high quality track fit, be consistent with origination from the primary pp interaction in the event, and be separated by at least $\Delta R = 0.5$ from the trigger muon. No isolation requirement is made on the tau muon. Overall, the trigger and tau muon quality criteria are similar, but the tau muon criteria are optimized for low p_T muons in a crowded detector environment, while instead the trigger muon criteria are optimized for high p_T isolated muons. More details on the performance of both selections can be found in Ref. [36].

Hadronically decaying tau leptons are reconstructed via the hadron plus strips (HPS) algorithm [37], which reconstructs one-prong (including leptonic decays), one-prong + one π^0, and three-prong decay modes. HPS taus are seeded from anti-k_T jets [38] with R parameter 0.5. For each jet, tau candidates are built from the jet constituents according to criteria that include consistency with the primary pp interaction vertex, consistency with the π^0 mass hypothesis, and minimization of the transverse energy sum of jet constituents not included in the tau candidate. All candidates are dropped from the final tau collection except the single candidate per jet most consistent with a real tau lepton decay based on these criteria.

Since the final state of interest in this analysis includes a pair of boosted taus from a or h decay, the HPS algorithm is modified to maintain high efficiency for overlapping taus. Prior to submitting the list of jet constituents to the tau reconstruction sequence, the seed jet constituents are checked for the presence of τ_μ candidates as defined above. Only jets that have at least one muon candidate passing the τ_μ criteria among their constituents are used to seed the HPS reconstruction. Within these selected jets, the muon is excluded from the reconstruction of the hadronic tau. An example di-tau pair undergoing this modified reconstruction is depicted in Figure 1. The HPS reconstruction then proceeds as above, and the resulting tau is required to have $p_T > 20$ GeV/c, $|\eta| < 2.3$, and be consistent with a one-prong (including leptonic decays), one-prong + one or two π^0, or three-prong decay. The HPS tau is also required to be isolated, meaning that the transverse energy sum (corrected for pileup) of electrons, photons, and hadrons in a cone of radius $\Delta R = 0.5$ around the tau must not exceed 1 GeV/c. The isolation energy sum does not include the identified tau muon. The ensemble of the tau muon and isolated HPS tau resulting from this selection are referred to collectively as a $\tau_\mu\tau_X$ object, as it is designed to reconstruct boosted $a/h \to \tau_\mu\tau_X$ decays. The HPS tau is referred to as τ_X because no anti-electron or anti-muon discriminators are applied to it; although taus decaying to electrons and muons can thus technically pass the HPS tau ID, it has been verified in simulation that the vast majority (∼97%) of taus passing this selection are indeed hadronically decaying taus. Because no isolation requirement is placed on the tau muon, it can be identified with high efficiency in the presence of a nearby tau. In $H \to aa/hh$ decays, the final state $\tau_\mu\tau_X$ object is expected to be isolated, and indeed the modified HPS tau reconstruction and isolation requirement is about as efficient for this decay as standard HPS and isolation requirements are for identifying $Z \to \tau\tau$ events. Figure 2 shows the efficiency for HPS taus to be reconstructed as one of the decay modes mentioned above and pass the isolation requirement for the case of boosted $\tau_\mu\tau_X$ pairs from simulated WH signal events and simulated $Z \to \tau\tau$ events.

Missing transverse energy $\not{E}_T$ is defined as the negative vectorial sum of the transverse mo-

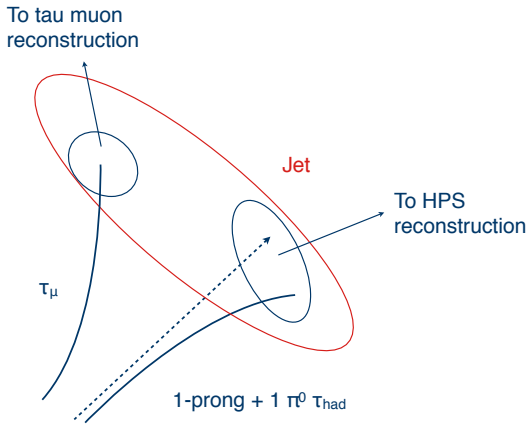

Figure 1: Boosted di-tau pair reconstruction.

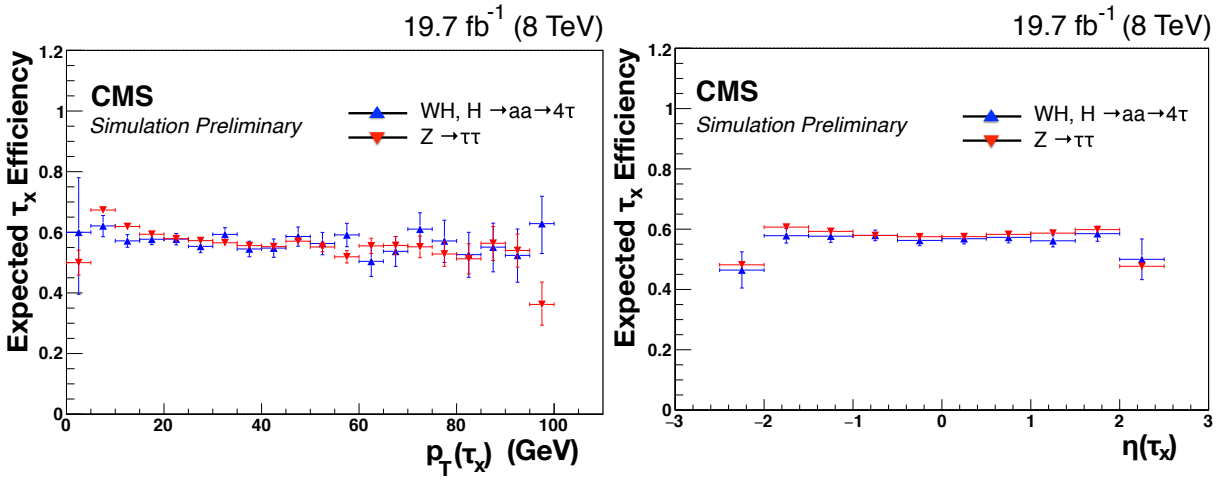

Figure 2: MC simulation prediction of the efficiency for HPS taus to be reconstructed as one of the decay modes mentioned in the text and pass the isolation requirement as a function of p_{T} (left) and η (right). Blue: WH $\rightarrow 4\tau$. Red: Z $\rightarrow \tau\tau$.

menta of jets, electrons, photons, taus, muons, and otherwise unclustered calorimeter hits. Jets are corrected for pileup, the underlying event, and nonuniformity of response over p_T and η [39]. Transverse mass M_T is defined as $\sqrt{2p_T^{\mu_{trg}} \not{E}_T (1 - \cos\Delta\phi(\mu_{trg}, \not{E}_T))}$ and is used in this analysis to distinguish the W associated production mode (high M_T) from the gluon fusion and VBF production modes (low M_T).

Jets are identified as b jets or light jets based on a multivariate discriminator that exploits the longer lifetime of B hadrons. To count as a b jet, the output of the combined secondary vertex (CSV) multivariate discriminator [40] must be greater than or equal to 0.679.

This analysis uses a data sample of 19.7 fb^{-1} collected by the CMS detector at a center-of-mass energy of 8 TeV. Events are triggered by the presence of at least one muon with $p_T > 24$ GeV/c reconstructed in the muon chambers ($|\eta| < 2.1$). The isolation requirement employed by the trigger is generally looser than that of the "trigger muon" reconstruction software, and for reasons of processing speed the trigger isolation calculation is based on calorimeter towers rather than particle flow objects.

Events are required to contain at least one particle flow reconstructed muon passing the trigger muon ID, matched within $\Delta R = 0.1$ to the object reconstructed in the high level trigger (HLT) system firing `HLT_IsoMu24_eta2p1`. The high level trigger and "trigger muon" ID are designed to reconstruct the high p_T isolated muon from W decay in the WH associated production mode, and also has high efficiency for the low p_T tau decay muons in the gluon fusion and VBF production modes when the taus from (pseudo)scalar decay are required to be well separated. Figure 3 shows the HLT efficiency for muons passing the trigger muon ID in both the WH and gluon fusion production modes. In both modes, the trigger muon ID includes the nearby lepton non-overlap requirement.

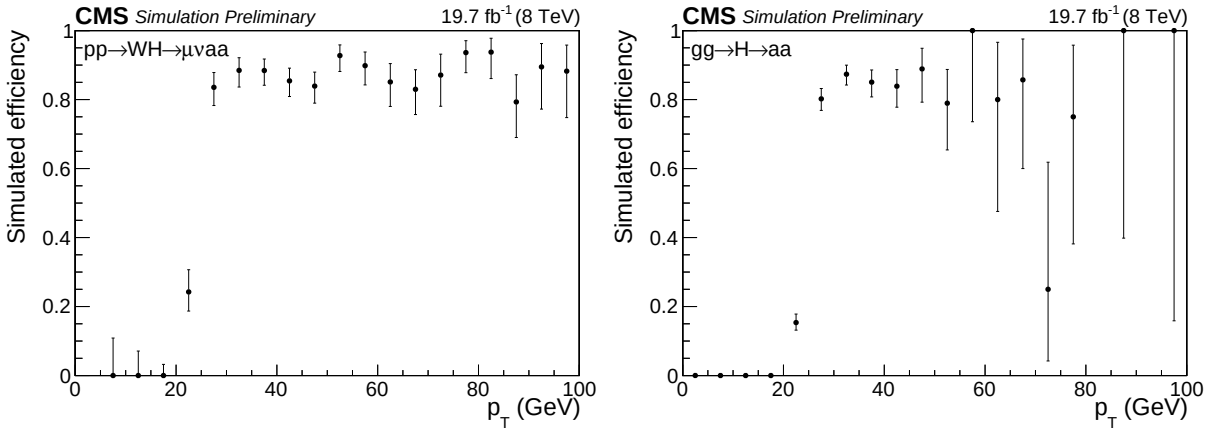

Figure 3: MC simulation prediction of efficiency for reconstructed muons passing the trigger muon ID to fire `HLT_IsoMu24_eta2p1`. Efficiencies were measured in MC events where the Higgs is produced via the (left) WH and (right) gluon fusion channels.

This analysis requires at least one $\tau_\mu\tau_X$ object, which reconstructs a single $a/h \to \tau\tau$ decay, is required per event. No requirement is imposed to identify the second $a/h \to \tau\tau$ decay in order to maintain higher signal acceptance. The $\tau_\mu\tau_X$ object consists of a muon, one or three other charged particle tracks, and zero or more neutral hadrons, and could therefore arise from misidentifying the decay products of a bottom quark jet. To further distinguish $\tau_\mu\tau_X$ objects, the seed jet of the HPS tau (excluding any identified tau muons) is required to be inconsistent with a b jet.

After the selections described above, the main backgrounds to this search are Drell-Yan di-muon pairs (one muon passes the trigger muon ID and the other passes the tau muon ID), $W \rightarrow \mu\nu$ + jets (the muon passes the trigger muon ID and the jet fakes the $\tau_\mu\tau_X$ object), $t\bar{t}$ di-muons (one muon passes the trigger muon ID and the other passes the tau muon ID), semileptonic $t\bar{t}$ (the muon passes the trigger muon ID and a b jet fakes the $\tau_\mu\tau_X$ object), and QCD b jets (a muon from one jet passes the trigger muon ID and another jet fakes the $\tau_\mu\tau_X$ object). In order to reduce the Drell-Yan background, the trigger muon and tau muon are required to have the same charge. To minimize all jet fake backgrounds, the tau muon and HPS tau are required to have opposite charge. Finally, events are classified into two analysis bins: $M_T \leq 50$ GeV/c^2, in which gluon fusion production accounts for ∼85% of the expected signal, VBF accounts for another 10%, and associated production accounts for the rest; and $M_T > 50$ GeV/c^2, in which gluon fusion and WH production each account for ∼40% of the expected signal and ZH and VBF account for the rest.

3 Search Strategy

The new physics signal under study is characterized by the presence of a resonance in the mass $\tau_\mu\tau_X$ spectrum. Even though the tau decays cannot be fully reconstructed due to the neutrino decay products, the visible di-tau mass $m_{\mu+X}$ distribution can still be used to discriminate the signal from Standard Model backgrounds, the latter tending to peak at very low values of $m_{\mu+X}$ (typically < 2 GeV/c^2). Visible di-tau mass is defined as the invariant mass of the tau muon and HPS tau objects described in Sec. 2. Figure 4 shows the distribution of $m_{\mu+X}$ after the event selection has been applied for the four Higgs production mechanisms considered and predictions of all backgrounds discussed in Sec. 2. While the signals have broad peaks around 4 GeV/c^2 and above due to the decay of the massive (pseudo)scalar, the backgrounds, due mainly to jets with muon decays, peak at lower values and fall off sharply.

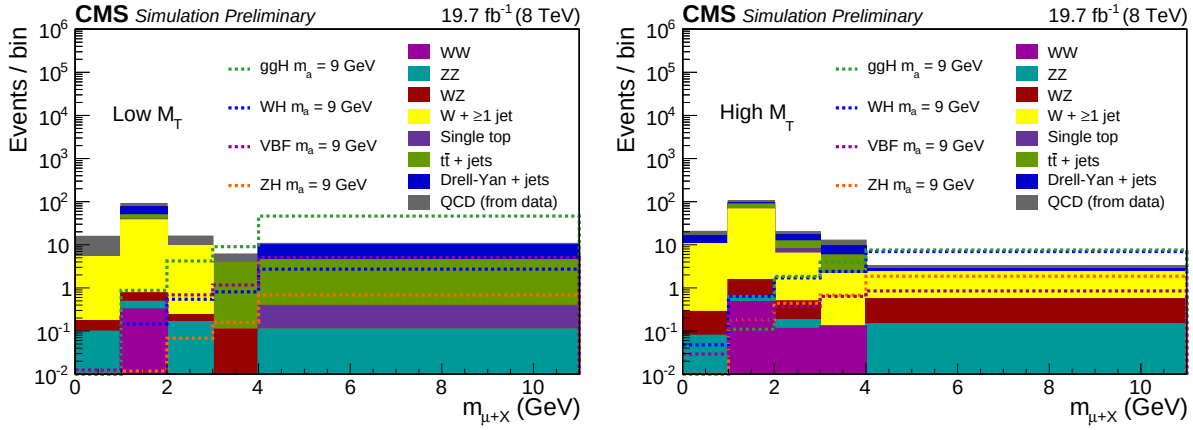

Figure 4: $m_{\mu+X}$ distribution after the preselection has been applied for the four Higgs production mechanisms considered and predictions of all backgrounds discussed in Sec. 2. Here, the QCD multi-jet background (gray) is predicted from data as described in Section 4, while other background predictions are from simulation (normalized to 19.7 fb^{-1}). Overflows are contained in the last bin. (left) Low-M_T bin. (right) High-M_T bin.

The analysis has been designed as a blinded counting experiment in the signal region ("region A", cf. Figure 5) defined by the cuts described in Sec. 2 plus $m_{\mu+X} > 4$ GeV/c^2. The dominant jet fake background shape is taken from control samples defined from the HPS tau isolation

sideband, and normalized to data passing all the cuts described in Sec. 2, but in the signal-depleted subsample with $m_{\mu+X} \leq 2$ GeV/c^2.

4 Background Estimation

Given the shape of the background $m_{\mu+X}$ distribution, the background yield in the signal region $m_{\mu+X} \geq 4$ GeV/c^2 can be estimated by normalizing the shape to the data yield in the background-dominated window $m_{\mu+X} < 2$ GeV/c^2. The background shape itself is estimated from data events with $m_{\mu+X} \geq 0$ satisfying all signal selections, except that the tau isolation is required to be between 1 and 5 GeV/c. The restriction on maximum tau isolation insures similarity between the tau p_T distributions of the signal and control samples, as the tau p_T is correlated to $m_{\mu+X}$ for jets faking taus. As tau isolation is a good discriminator between real taus and jets, the inverted isolation requirement implies that this control sample should be enriched in isolated muon + jet events. It was explicitly checked in simulated samples of W + jets and $t\bar{t}$ events, in which the the $\tau_\mu\tau_X$ candidate arises from misidentified jets, that events with non-isolated taus have the same kinematics as those of the signal sample.

The background shape is estimated from three different control samples with tau isolation between 1 and 5 GeV/c in order to evaluate the systematic uncertainty: data events passing all other signal selections ("region B data", cf. Figure 5); simulated Drell-Yan, W + jets, $t\bar{t}$, and di-boson events passing all other signal selections ("region B simulation"); and data events passing all other signal selections, but with trigger muon relative isolation $\geq$0.12 and no requirement on nearby lepton isolation ("region D data", cf. Figure 5). To obtain the three independent estimated background yields, the shape from each sample is scaled by $N_A^{data}(m_{\mu+X} < 2$ GeV/$c^2)/N_{est}(m_{\mu+X} < 2$ GeV/$c^2)$, where $N_A^{data}(m_{\mu+X} < 2$ GeV/$c^2)$ is the number of events in the signal region A (cf. Fig. 5) with $m_{\mu+X} < 2$ GeV/c^2 and $N_{est}(m_{\mu+X} < 2$ GeV/$c^2)$ is the number of events in the non-isolated tau control sample with $m_{\mu+X} < 2$ GeV/c^2. The chosen normalization region $m_{\mu+X} < 2$ GeV/c^2 is background dominated, as shown in Fig. 4.

Region B data consists of Drell-Yan, W, $t\bar{t}$, diboson, and QCD multi-jet contributions, and is expected to model the background composition in region A. To illustrate the individual backgrounds, Fig. 4 shows simulations of the Drell-Yan, W, $t\bar{t}$, and diboson contributions, while the QCD multi-jet contribution is predicted from data. The shape of the $m_{\mu+X}$ distribution due to QCD comes from region C data (cf. Fig. 5), defined as passing all region A signal selections except failing the trigger muon isolation requirement. Region C contains di-jet events where the jets have at least one muon decay. It is scaled by $[N_B^{data}(m_{\mu+X} < 3$ GeV/$c^2) - N_B^{sim}(m_{\mu+X} < 3$ GeV/$c^2)]/N_D^{data}(m_{\mu+X} < 3$ GeV/$c^2)$, where $N_B^{data}(m_{\mu+X} < 3$ GeV/$c^2)$ is the number of data events in the control region B (cf. Fig. 5) with $m_{\mu+X} < 3$ GeV/c^2, $N_B^{sim}(m_{\mu+X} < 3$ GeV/$c^2)$ is the number of simulated Drell-Yan, W, $t\bar{t}$, and diboson events estimated for 19.7 fb^{-1} in region B with $m_{\mu+X} < 3$ GeV/c^2, and $N_D^{data}(m_{\mu+X} < 3$ GeV/$c^2)$ is the number of data events in the QCD-dominated control region D with $m_{\mu+X} < 3$ GeV/c^2. The scaling assumes that QCD is a contribution in region B that is not simulated, so the difference between the data observed and the simulation in region B is due to QCD. This is confirmed in detailed comparisons of region B data to simulation.

The uncertainty on the total background estimate is dominated by imperfect knowledge of the jet$\rightarrow \tau$ fake background composition in region A. There are several mechanisms for $\tau_\mu\tau_X$ misidentification, for example jets with semi-leptonic decays, jets with double semi-leptonic decays, resonances in b jet decays, or light jets. The relative composition of background events of each type in regions A and B may be somewhat different, and it is impractical to simulate

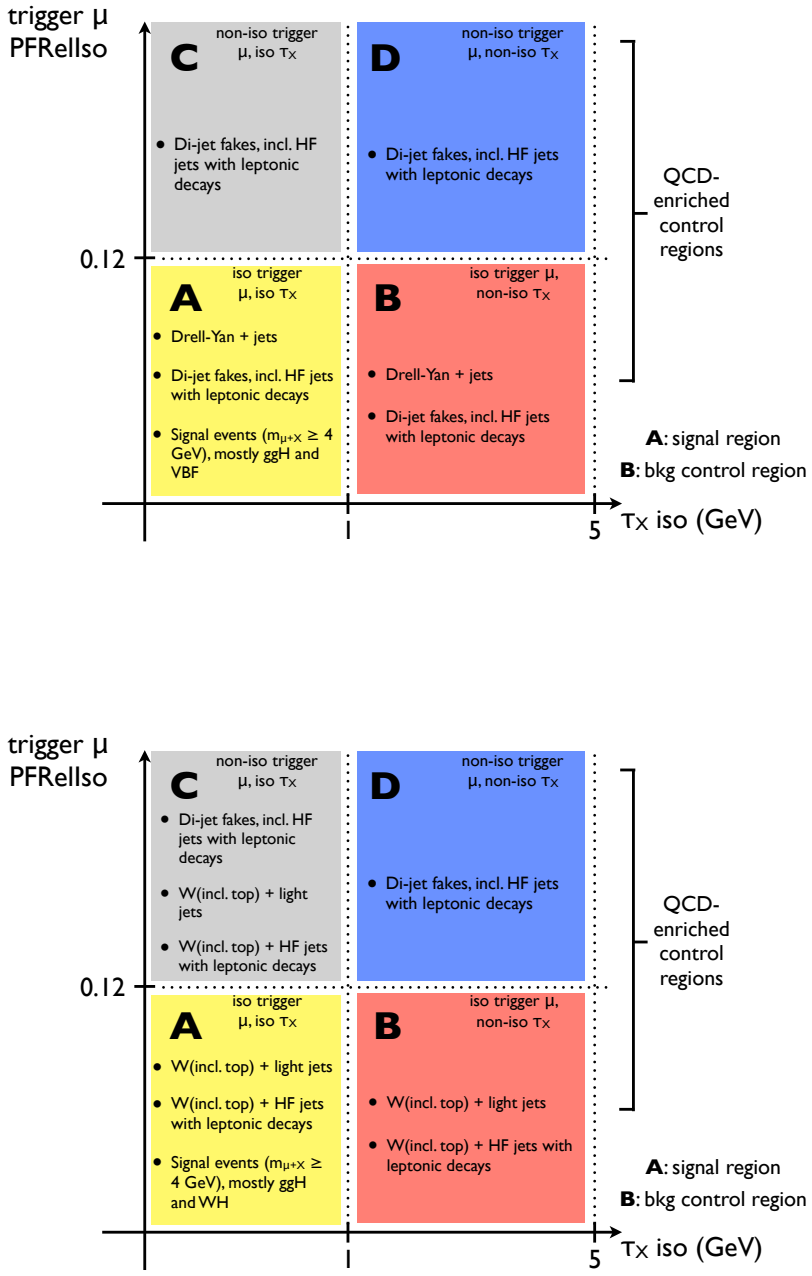

Figure 5: Schematic description of the four data samples used in this analysis. Events in region A are required to pass all analysis cuts detailed in Sec. 2, while events in regions B, C, and D have either or both of the τ_X or μ_{trg} isolation reversed. (Top) Low M_T. (Bottom) High M_T.

the backgrounds to the required statistical precision. To evaluate this effect, the background is estimated independently from the three distinct samples discussed above, and the final background prediction is taken as the arithmetic mean of the estimates from the three samples. The high(low) systematic uncertainty is taken as the difference between the largest(smallest) of the three plus(minus) its statistical error and the average, thus covering all three measurements at 68% C.L. The final background estimate in the low- and high-M_{T} bins with all errors is

- Low-M_{T}: 5.41 $\pm$ 1 (stat) +4.2/-4.6 (syst)
- High-M_{T}: 6.08 $\pm$ 1.6 (stat) +3.7/-3.6 (syst)

Figure 6 shows the jet fake background estimate, the boosted di-muon and di-tau resonances background estimate, the data, and the four signal production models.

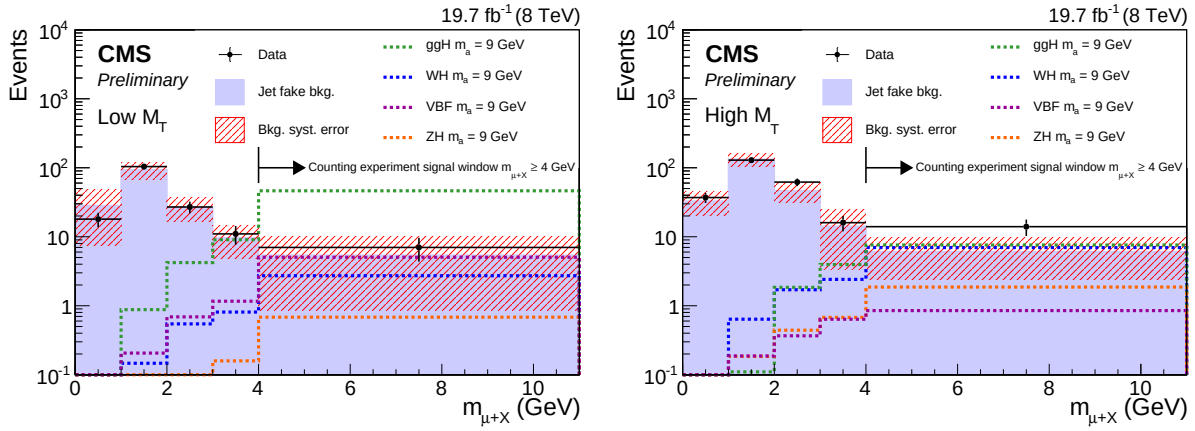

Figure 6: Comparison of $m_{\mu+\mathrm{X}}$ distributions for observed data in region A (black curve) and the jet fake background estimate (purple) from the average of shapes taken from region B data, region B simulation, and region D data, each normalized using the signal-poor sideband $m_{\mu+\mathrm{X}} < 2$ GeV/c^2; the signal region is $m_{\mu+\mathrm{X}} > 4$ GeV/c^2. Predicted signal distributions (dotted lines) for each of the four Higgs production mechanisms are also shown; the curves are normalized to 19.7 fb^{-1} assuming SM Higgs production cross sections and $BR(\mathrm{H} \to \mathrm{aa/hh})BR^2(\mathrm{a/h} \to \tau\tau)$ = 100%. The red shaded band shows the background systematic error described in the text. (left) Low M_{T}. (right) High M_{T}.

5 Results

With the event count in the signal window compatible with the standard model background prediction, the results are interpreted as upper limits on $BR(\mathrm{H} \to \mathrm{aa/hh})BR^2(\mathrm{a/h} \to \tau\tau)$ assuming standard model cross sections for ggH, WH, ZH, and VBF production. Upper limits are calculated using the LHC-style CL$_{\mathrm{S}}$ technique [41], in which the profile likelihood variable is the test statistic and signal hypothesis rejection is based on a modified frequentist probability in order to reduce the rejection of signals to which the experiment has weak sensitivity. The profile likelihood test statistic uses best-fit values of the nuisance parameters (experimental uncertainties) simultaneously determined from a fit of the signal + background likelihood function to the data. Table 1 lists the uncertainties considered in this analysis. All uncertainties are modeled as log-normal functions in the construction of the full model likelihood, where the expectation value is 1 and the variance is related to the magnitude of the uncertainty.

Signal acceptance is calculated from the simulated samples described in Sec. 2 for WH m_{a} =

Table 1: Systematic uncertainties considered in this analysis. The first column lists the source of the uncertainty and the second column indicates the magnitudes in terms of its effect on the signal or background yield prediction. Unless specified otherwise, the uncertainties are taken to be symmetric.

Uncertainty	Magnitude	
	$M_T \leq 50$ GeV/c^2	$M_T > 50$ GeV/c^2
Luminosity	2.6%	2.6%
HLT	(0.2-4.2)%	(0.2-4.2)%
Trigger muon ID	0.5%	0.5%
Trigger muon isolation	(0.2-3.8)%	(0.2-3.8)%
Trigger muon lepton isolation	10%	10%
Tau muon ID	1.5%	1.5%
HPS tau ID	6%	6%
HPS tau charge mis-ID	-1%/+2%	-1%/+2%
Background model	-84%/+78%	-59/+61%
b veto	<9.4%	<8.5%
M_T scale	<4.2%	<9.3%
VBF extrapolation	23%	25%
ZH extrapolation	19%	24%

$\{5, 7, 9, 11, 13, 15\}$ GeV/c^2, ggH $m_a = \{5, 7, 9, 11, 13, 15\}$ GeV/c^2, ZH $m_a = 9$ GeV/c^2, and VBF $m_a = 9$ GeV/c^2. For ZH $m_a = \{5, 7, 11, 13, 15\}$ GeV/c^2, the acceptance is estimated as $A^i_{ZH} = (A^{9\,\mathrm{GeV}/c^2}_{ZH} / A^{9\,\mathrm{GeV}/c^2}_{WH}) \times A^i_{WH}$, where $i \in \{5, 7, 11, 13, 15\}$ GeV/c^2, $A^{9\,\mathrm{GeV}/c^2}_{ZH}(A^{9\,\mathrm{GeV}/c^2}_{WH})$ is the acceptance calculated from the simulated ZH (WH) sample with $m_a = 9$ GeV/c^2, and A^i_{WH} is the acceptance calculated from the simulated WH sample with $m_a = i$. Similarly, for VBF $m_a = \{5, 7, 11, 13, 15\}$ GeV/c^2, the acceptance is estimated as $A^i_{VBF} = (A^{9\,\mathrm{GeV}/c^2}_{ggH} / A^{9\,\mathrm{GeV}/c^2}_{VBF}) \times A^i_{ggH}$, where $i \in \{5, 7, 11, 13, 15\}$ GeV/c^2, $A^{9\,\mathrm{GeV}/c^2}_{VBF}(A^{9\,\mathrm{GeV}/c^2}_{ggH})$ is the acceptance calculated from the simulated VBF(ggH) sample with $m_a = 9$ GeV/c^2, and A^i_{ggH} is the acceptance calculated from the simulated ggH sample with $m_a = i$. Table 2 shows the expected number of events and assumed cross section for each signal sample, the background expectation, and the observation for the two analysis regions. The expected signal acceptance is corrected using p_T- and $|\eta|$-dependent scale factors to account for known differences in the b veto efficiency between data and simulation [40].

In the low and high M_T regions separately, 95% C.L. upper limits on the branching ratio product $BR(H \to aa/hh)BR^2(a/h \to \tau\tau) \equiv BR(H \to aa \to 4\tau)$ were calculated for the sum of contributions from all production mechanisms considered, under the assumption that the mass of the H is 125 GeV/c^2 and that the cross-sections for all of its production mechanisms are SM-like [42]. Plots of the expected limits (median, $\pm 1\sigma$, and $\pm 2\sigma$) and observed limit for the low-M_T bin, high-M_T bin, and a combination of the two bins at different m_a points are shown in Figure 7. For the combination, all systematic errors were treated as 100% correlated except for the background uncertainties in the two bins, which were treated as uncorrelated. The limits are reported in terms of the total branching ratio $BR(H \to aa \to 4\tau)$, assuming standard model Higgs production cross sections.

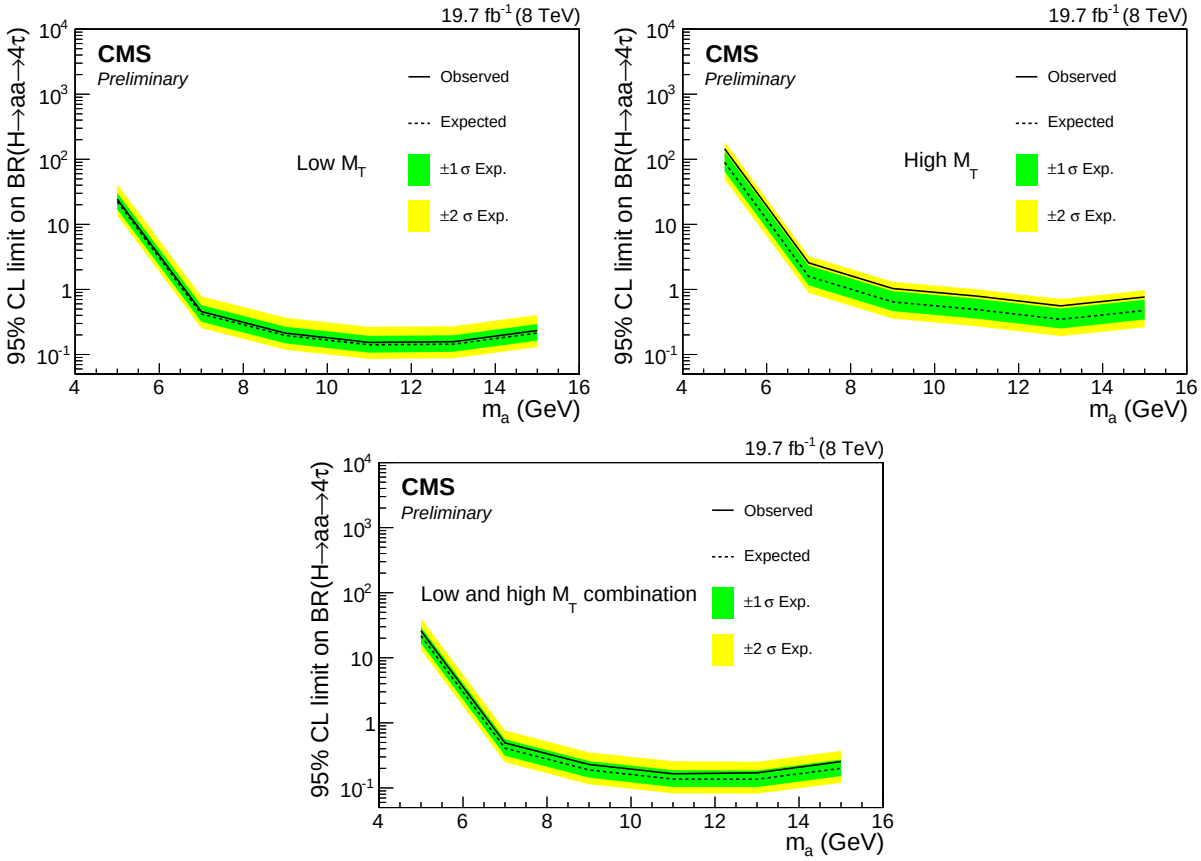

Figure 7: Observed 95% C.L. limits (solid black curve) on the branching ratio $BR(\mathrm{H} \rightarrow \mathrm{aa} \rightarrow 4\tau)$, compared to expected limits (dotted black curve, with $\pm 1\sigma$ bands in green and $\pm 2\sigma$ bands in yellow) at pseudoscalar mass points m_{a} = 5 through 15 GeV/c^2. (Top left) $M_{\mathrm{T}} \leq 50$ GeV/c^2. (Top right) $M_{\mathrm{T}} > 50$ GeV/c^2. (Bottom) Combination of low and high M_{T} bins.

Table 2: Predictions for signal yields from each generated pseudoscalar mass point, predictions for SM backgrounds, and observed events in data in the low and high M_T regions. Only statistical errors are shown.

		Cross section (pb)	$M_T \leq 50$ GeV/c^2	$M_T > 50$ GeV/c^2
WH	$m_a = 5$ GeV/c^2	0.2296	0.11 ± 0.05	0.10 ± 0.04
	$m_a = 7$ GeV/c^2		1.5 ± 0.2	3.8 ± 0.3
	$m_a = 9$ GeV/c^2		2.7 ± 0.2	7.0 ± 0.3
	$m_a = 11$ GeV/c^2		4.2 ± 0.3	8.8 ± 0.4
	$m_a = 13$ GeV/c^2		3.5 ± 0.2	9.9 ± 0.4
	$m_a = 15$ GeV/c^2		3.6 ± 0.2	8.4 ± 0.4
ggH	$m_a = 5$ GeV/c^2	19.27	0.3 ± 0.2	0
	$m_a = 7$ GeV/c^2		21 ± 2	1.9 ± 0.6
	$m_a = 9$ GeV/c^2		46 ± 3	8 ± 1
	$m_a = 11$ GeV/c^2		64 ± 3	11 ± 1
	$m_a = 13$ GeV/c^2		63 ± 3	18 ± 2
	$m_a = 15$ GeV/c^2		41 ± 3	11 ± 1
ZH	$m_a = 5$ GeV/c^2	0.4153	0.03 ± 0.01	0.03 ± 0.01
	$m_a = 7$ GeV/c^2		0.38 ± 0.04	1.0 ± 0.1
	$m_a = 9$ GeV/c^2		0.68 ± 0.05	1.9 ± 0.1
	$m_a = 11$ GeV/c^2		1.1 ± 0.05	2.3 ± 0.1
	$m_a = 13$ GeV/c^2		0.88 ± 0.06	2.7 ± 0.1
	$m_a = 15$ GeV/c^2		0.91 ± 0.06	2.3 ± 0.1
VBF	$m_a = 5$ GeV/c^2	1.578	0.03 ± 0.02	0
	$m_a = 7$ GeV/c^2		2.3 ± 0.2	0.22 ± 0.06
	$m_a = 9$ GeV/c^2		5.1 ± 0.3	0.9 ± 0.1
	$m_a = 11$ GeV/c^2		7.0 ± 0.4	1.2 ± 0.1
	$m_a = 13$ GeV/c^2		6.9 ± 0.4	2.0 ± 0.2
	$m_a = 15$ GeV/c^2		4.5 ± 0.3	1.3 ± 0.2
SM Background			5.41 ± 1 (stat) $^{+4.2}_{-4.6}$ (syst)	6.08 ± 1.6 (stat) $^{+3.7}_{-3.6}$ (syst)
Data (observed)			7	14

6 Conclusions

A search for evidence of the decay $H \to aa/hh \to 4\tau$ was performed using 19.7 fb^{-1} of data collected by the CMS experiment at the LHC. Such a signature, in which an SM-like H decays to two light (pseudo)scalars in the mass range 5−15 GeV/c^2, is of interest in light of the significant branching ratio allowed by the latest experimental constraints for unseen H decays. The data were found to be compatible with standard model predictions of a single 125 GeV/c^2 Higgs boson and no others. Upper limits on $BR(H \to aa/hh)BR^2(a/h \to \tau\tau)$, assuming standard model production of the 125 GeV/c^2 Higgs via the ggH, WH, ZH, and VBF modes, were set. This result is the first of its kind for the 4τ final state at the LHC. For a 9 GeV/c^2 (pseudo)scalar, an upper limit of 21% was set on $BR(H \to 4\tau)$, which should be compared with the indirect limit of 39% on various models that include light (pseudo)scalars with a high branching ratio to taus.

References

[1] ATLAS Collaboration, "Updated coupling measurements of the Higgs boson with the ATLAS detector using up to 25 fb^{-1} of proton-proton collision data", ATLAS Note ATLAS-CONF-2014-009, 2014.

[2] CMS Collaboration, "Combination of standard model Higgs boson searches and measurements of the properties of the new boson with a mass near 125 GeV", CMS Physics Analysis Summary CMS-PAS-HIG-13-005, 2013.

[3] ATLAS Collaboration, "Measurements of Higgs boson production and couplings in diboson final states with the ATLAS detector at the LHC", *Phys. Lett. B* **726** (2013) 88, doi:10.1016/j.physletb.2013.08.010, arXiv:1307.1427.

[4] ATLAS Collaboration, "Observation of a new particle in the search for the Standard Model Higgs boson with the ATLAS detector at the LHC", *Phys. Lett. B* **716** (2012) 1, doi:10.1016/j.physletb.2012.08.020, arXiv:1207.7214.

[5] CMS Collaboration, "Observation of a new boson at a mass of 125 GeV with the CMS experiment at the LHC", *Phys. Lett. B* **716** (2012) 30, doi:10.1016/j.physletb.2012.08.021, arXiv:1207.7235.

[6] G. Belanger et al., "Global fit to Higgs signal strengths and couplings and implications for extended Higgs sectors", *Phys. Rev. D.* **88** (2013) 075008, doi:10.1103/PhysRevD.88.075008, arXiv:1306.2941.

[7] R. Dermisek and J. F. Gunion, "Escaping the large fine tuning and little hierarchy problems in the next to minimal supersymmetric model and $h \to aa$ decays", *Phys. Rev. Lett.* **95** (2005) 041801, doi:10.1103/PhysRevLett.95.041801, arXiv:hep-ph/0502105.

[8] R. Dermisek and J. F. Gunion, "The NMSSM Close to the R-symmetry Limit and Naturalness in $h \to aa$ Decays for $m(a) < 2m(b)$", *Phys. Rev. D* **75** (2007) 075019, doi:10.1103/PhysRevD.75.075019, arXiv:hep-ph/0611142.

[9] S. Chang, R. Dermisek, J. F. Gunion, and N. Weiner, "Nonstandard Higgs Boson Decays", *Ann. Rev. Nucl. Part. Sci.* **58** (2008) 75, doi:10.1146/annurev.nucl.58.110707.171200, arXiv:0801.4554.

[10] D. Curtin et al., "Exotic decays of the 125 GeV Higgs boson", *Phys. Rev. D* **90** (2014) 075004, doi:10.1103/PhysRevD.90.075004, arXiv:1312.4992.

[11] A. Celis, V. Ilisie, and A. Pich, "LHC constraints on two-Higgs doublet models", *J. High Energy Phys.* **1307** (2013) 053, doi:10.1007/JHEP07(2013)053, arXiv:1302.4022.

[12] B. Grinstein and P. Uttayarat, "Carving Out Parameter Space in Type-II Two Higgs Doublets Model", *J. High Energy Phys.* **1306** (2013) 094, doi:10.1007/JHEP06(2013)094, arXiv:1304.0028.

[13] B. Coleppa, F. Kling, and S. Su, "Constraining Type II 2HDM in Light of LHC Higgs Searches", *J. High Energy Phys.* **1401** (2014) 161, doi:10.1007/JHEP01(2014)161, arXiv:1305.0002.

[14] C.-Y. Chen, S. Dawson, and M. Sher, "Heavy Higgs Searches and Constraints on Two Higgs Doublet Models", *Phys. Rev. D* **88** (2013) 015018, doi:10.1103/PhysRevD.88.015018, arXiv:1305.1624.

[15] N. Craig, J. Galloway, and S. Thomas, "Searching for Signs of the Second Higgs Doublet", (2013). arXiv:1305.2424.

[16] L. Wang and X.-F. Han, "Status of the aligned two-Higgs-doublet model confronted with the Higgs data", *J. High Energy Phys.* **1404** (2014) 128, doi:10.1007/JHEP04(2014)128, arXiv:1312.4759.

[17] J. Baglio, O. Eberhardt, U. Nierste, and M. Wiebusch, "Benchmarks for Higgs Pair Production and Heavy Higgs Searches in the Two-Higgs-Doublet Model of Type II", *Phys. Rev. D* **90** (2014) 015008, doi:10.1103/PhysRevD.90.015008, arXiv:1403.1264.

[18] B. Dumont, J. F. Gunion, Y. Jiang, and S. Kraml, "Constraints on and future prospects for Two-Higgs-Doublet Models in light of the LHC Higgs signal", *Phys. Rev. D* **90** (2015) 035021, doi:10.1103/PhysRevD.90.035021, arXiv:1405.3584.

[19] S. King, M. Muehlleitner, R. Nevzorov, and K. Walz, "Natural NMSSM Higgs Bosons", *Nucl. Phys. B* **870** (2013) 323, doi:10.1016/j.nuclphysb.2013.01.020, arXiv:1211.5074.

[20] J. Cao et al., "A light Higgs scalar in the NMSSM confronted with the latest LHC Higgs data", *J. High Energy Phys.* **1311** (2013) 018, doi:10.1007/JHEP11(2013)018, arXiv:1309.4939.

[21] N. D. Christensen, T. Han, Z. Liu, and S. Su, "Low-Mass Higgs Bosons in the NMSSM and Their LHC Implications", *J. High Energy Phys.* **1308** (2013) 019, doi:10.1007/JHEP08(2013)019, arXiv:1303.2113.

[22] D. G. Cerdeno, P. Ghosh, and C. B. Park, "Probing the two light Higgs scenario in the NMSSM with a low-mass pseudoscalar", *J. High Energy Phys.* **1306** (2013) 031, doi:10.1007/JHEP06(2013)031, arXiv:1301.1325.

[23] G. Chalons and F. Domingo, "Analysis of the Higgs potentials for two doublets and a singlet", *Phys. Rev. D* **86** (2012) 115024, doi:10.1103/PhysRevD.86.115024, arXiv:1209.6235.

[24] A. Ahriche, A. Arhrib, and S. Nasri, "Higgs Phenomenology in the Two-Singlet Model", *J. High Energy Phys.* **1402** (2014) 042, doi:10.1007/JHEP02(2014)042, arXiv:1309.5615.

[25] S. F. King, M. Muehlleitner, R. Nevzorov, and K. Walz, "Discovery Prospects for NMSSM Higgs Bosons at the High-Energy Large Hadron Collider", *Phys. Rev. D* **90** (2014) 095014, doi:10.1103/PhysRevD.90.095014, arXiv:1408.1120.

[26] CMS Collaboration, "Search for a light NMSSM Higgs boson produced in supersymmetric cascades and decaying into a b-quark pair", CMS Physics Analysis Summary CMS-PAS-HIG-14-030, 2015.

[27] CMS Collaboration, "A Search for Pair Production of New Light Bosons Decaying into Muons", (2015). arXiv:1506.00424. Submitted to *Phys. Lett. B*.

[28] CMS Collaboration, "Search for a light pseudoscalar Higgs boson in the dimuon decay channel in pp collisions at $\sqrt{s} = 7$ TeV", *Phys. Rev. Lett.* **109** (2012) 121801, doi:10.1103/PhysRevLett.109.121801, arXiv:1206.6326.

[29] R. Dermisek and J. F. Gunion, "Direct production of a light CP-odd Higgs boson at the Tevatron and LHC", *Phys. Rev. D* **81** (2010) 055001, doi:10.1103/PhysRevD.81.055001, arXiv:0911.2460.

[30] CMS Collaboration, "The CMS experiment at the CERN LHC", *J. Instrum.* **3** (2008) S08004, doi:10.1088/1748-0221/3/08/S08004.

[31] J. Alwall et al., "MadGraph 5: going beyond", *J. High Energy Phys.* **06** (2011) 128, doi:10.1007/JHEP06(2011)128, arXiv:1106.0522.

[32] Sjöstrand, T. and Mrenna, S. and Skands, P., "PYTHIA 6.4 physics and manual", *J. High Energy Phys.* **0605** (2006) 026, doi:doi:10.1088/1126-6708/2006/05/026, arXiv:hep-ph/0603175.

[33] Z. Wąs, "TAUOLA the library for τ lepton decay, and KKMC/KORALB/KORALZ/... status report", *Nucl. Phys. Proc. Suppl.* **98** (2001) 96, doi:10.1016/S0920-5632(01)01200-2, arXiv:hep-ph/0011305.

[34] J. Allison et al., "Geant4 developments and applications", *IEEE Trans. Nucl. Sci.* **53** (2006) 270, doi:10.1109/TNS.2006.869826.

[35] CMS Collaboration, "Performance of electron reconstruction and selection with the CMS detector in proton-proton collisions at $\sqrt{s} = 8$ TeV", *J. Instrum.* **10** (2015) P06005, doi:10.1088/1748-0221/10/06/P06005, arXiv:1502.02701.

[36] CMS Collaboration, "Performance of CMS muon reconstruction in pp collision events at $\sqrt{s} = 7$ TeV", *J. Instrum.* **7** (2012) P10002, doi:doi:10.1088/1748-0221/7/10/P10002, arXiv:1206.4071.

[37] CMS Collaboration, "Performance of τ-lepton reconstruction and identification in CMS", *J. Instrum.* **7** (2012) P01001, doi:10.1088/1748-0221/7/01/P01001, arXiv:1109.6034.

[38] M. Cacciari, G. P. Salam, and G. Soyez, "The anti-k_{T} jet clustering algorithm", *J. High Energy Phys.* **0804** (2008) 063, doi:10.1088/1126-6708/2008/04/063, arXiv:0802.1189.

[39] CMS Collaboration, "Determination of jet energy calibration and transverse momentum resolution in CMS", *J. Instum.* **7** (2011) P11002, doi:10.1088/1748-0221/6/11/P11002, arXiv:1107.4277.

[40] CMS Collaboration, "Identification of b-quark jets with the CMS experiment", *J. Instrum.* **8** (2013) P04013, doi:doi:10.1088/1748-0221/8/04/P04013, arXiv:1211.4462.

[41] CMS, ATLAS, and LHC Higgs Combination Group Collaboration, "Procedure for the LHC Higgs boson search combination in Summer 2011", CMS Note CMS-NOTE-2011-005, ATL-PHYS-PUB-2011-11, 2011.

[42] LHC Higgs Cross Section Working Group Collaboration, "Handbook of LHC Higgs Cross Sections: 3. Higgs Properties", (2013). arXiv:1307.1347.